Dynamic characteristics and seismic behavior of prefabricated steel stairs in a full-scale five-story building shake table test program

Xiang Wang[1], Rodrigo Astroza[1,2], Tara C. Hutchinson[1,*,†], Joel P. Conte[1] and
José I. Restrepo[1]

[1]*Department of Structural Engineering, University of California at San Diego, La Jolla, CA 92093, U.S.A.*
[2]*Facultad de Ingenieria y Ciencias Aplicadas, Universidad de los Andes, Santiago, Chile*

SUMMARY

This paper investigates the dynamic characteristics and seismic behavior of prefabricated steel stairs in a full-scale five-story building shake table test program. The test building was subjected to a suite of earthquake input motions and low-amplitude white noise base excitations first, while the building was isolated at its base, and subsequently while it was fixed to the shake table platen. This paper presents the modal characteristics of the stairs identified using the data recorded from white noise base excitation tests as well as the physical and measured responses of the stairs from the earthquake tests. The observed damage to the stairs is categorized into three distinct damage states and is correlated with the interstory drift demands of the building. These shake table tests highlight the seismic vulnerability of modern designed stair systems and in particular identifies as a key research need the importance of improving the deformability of flight-to-building connections. Copyright © 2015 John Wiley & Sons, Ltd.

1. INTRODUCTION

Stairs are a primary means of egress in most buildings and therefore are critical to building accessibility and survivability in the event of an emergency. They should remain operable following even a rare and strong-intensity earthquake and ensuing post-earthquake disasters to support occupant evacuation and recovery response [1]. However, the behavior of stairs is complex, and their response during an earthquake has been demonstrated to be poor in prior earthquakes [2–5]. This is largely due to the variability in spatial geometry (e.g., straight-run, scissors, and spiral), material (e.g., reinforced concrete, steel, and wood), and construction methods (e.g., cast-in-place, site-assembled, precast, or prefabricated). Each of these aspects significantly affect the structural behavior and integrity of stairs. For example, stairs in a scissor configuration are susceptible to twist as their structural form rises in elevation, whereas straight-run stairs will be significantly weaker orthogonal to the primary direction. Steel stairs tend to be more deformable and lighter than those constructed with reinforced concrete. In addition, some stairs (e.g., cast-in-place reinforced concrete stairs) may detrimentally interact with the supporting structure by acting as diagonal braces during lateral loading. These stiffer and heavier stairs may shift the centers of mass and stiffness of a building, and therefore inducing significant torsion to the building.

---

*Correspondence to: Tara C. Hutchinson, Department of Structural Engineering, University of California at San Diego, La Jolla, CA 92093.
†E-mail: tara@ucsd.edu

Regardless of these specifics, in US design practice, stairs are typically attached to their primary structure and span as a floor-to-floor system, and therefore, they are subjected to dynamic multi-support excitations during an earthquake. Although the seismic design forces for stairs can be readily determined from code provisions [6], detailing these floor-to-floor systems to remain damage-free during relative deformation between their upper and lower floors is difficult. The current state of practice often imposes specific provisions to one end of the stair (e.g., ductile or slotted connections and seismic gaps) to accommodate the anticipated floor-to-floor (interstory) relative drift. However, more commonly designers simply fix both the top and bottom of a stair system to the upper and lower floors of the supporting structure. This practice has demonstrated catastrophic results, as the stairs lack protection from large floor-to-floor relative displacements.

Numerous earthquakes documented these and other damage modes to stair systems (e.g., [2–5]). Severe damage and collapse of stairs were reported following the 2008 Wenchuan earthquake in China [4], the 2010 Maule earthquake in Chile (Figure 1(a)), and the 2011 Christchurch earthquake in New Zealand [2, 3] (Figure 1(b)). Stair damage in these earthquakes caused disruptions to building functionality, delayed rescue operations, and threatened safety.

Despite these and other evidence of the vulnerability of stairs and the implications related to stair damage, experimental studies on the seismic behavior of stair systems have occurred only in a few occasions [7, 8]. In the study of Simmons and Bull [8], quasi-static cyclic tests of three full-height reinforced concrete straight-run stair flights conforming to the New Zealand design code were conducted, whereas Higgins [7] performed tests of two full-sized prefabricated steel scissor stairs constructed in accordance with the US design standards. These studies advance the state of understanding regarding the seismic behavior of stair systems; however, they were both conducted in their isolated configuration using quasi-static cyclic loading to replicate earthquake floor drifts. Past research has also attempted to quantify the impact of a stair system on the building response (e.g., [9, 10]). These works have primarily focused on numerical simulations of system-level building models with and without stairs incorporated. To date, limited test data is available to validate findings of these and other numerical studies. Complementing these studies, system-level testing using earthquake motions is warranted. Such tests would capture the dynamic interaction between the stairs and the supporting structure as well as other nonstructural components. To the authors' knowledge, a seismic test program of a stair system as installed within a building has yet to be conducted.

To this end, a landmark full-scale five-story building, completely outfitted with a broad array of nonstructural components and systems, was tested on the Network for Earthquake Engineering Simulation Large High-Performance Outdoor Shake Table [11] at the University of California, San Diego

(a)   (b)

Figure 1. Stair damage in prior earthquakes: (a) crumbled exterior reinforced concrete stairs in the 2010 Maule earthquake and (b) damaged interior precast concrete stairs in the 2011 Christchurch earthquake.

(UCSD) in 2012 [12–14]. Within this test building, for the first time, a prefabricated steel stair system was installed at full scale, allowing investigation of system-level interactions between the primary structure and the stairs as well as interaction between the stairs and other nonstructural components. In this paper, the modal characteristics of the stair system identified using white noise (WN) base excitation test data are presented. In addition, the physical and measured responses of the stair system from the earthquake tests are reported. The observed damage to the stairs is categorized into three damage states and correlated with the peak interstory drift demands experienced by the test building.

2. SHAKE TABLE TEST PROGRAM

The full-scale five-story test building was constructed with cast-in-place reinforced concrete and designed to resist seismic loads with a pair of special moment frames in the direction of shaking (east-west direction) (Figure 2(a)). The design utilized ground motions developed for a site in Southern California, with the maximum considered earthquake (MCE) ground motion spectrum for a Site Class D (stiff) soil conditions, with a short-period spectral acceleration S_{MS} = 2.1 g and a one-second spectral acceleration S_{M1} = 1.4 g. The MCE level performance targets of 2.5% peak interstory drift ratio (PIDR) and maximum peak floor acceleration (PFA) between 0.7 and 0.8 g were selected during the conceptual design phase. As shown in Figure 2(b), the building had two bays in the longitudinal direction and one bay in the transverse direction, with a plan dimension of 11.0 × 6.6 m. Two moment resisting frames were placed in the east bay (north and south sides) in the longitudinal (shaking) direction, while two transverse shear walls were placed within the interior of the building to provide transverse lateral load resistance. The slabs were 204-mm thick cast-in-place concrete and incorporated two large openings, one on the northwest to accommodate a full-height elevator shaft and the other on the southeast for the stairs. The building floor-to-floor height was 4.3 m at each level, resulting in a total building height of 21.3 m above the foundation (Figure 2(c)).

The seismic test program comprised two phases, namely: (i) the building isolated at its base (BI) and subjected to seven earthquake input motions and (ii) the building fixed at its base (FB) and subjected to six earthquake input motions. In addition, low-amplitude WN base excitation tests were conducted at various stages during the test program to facilitate the identification of the dynamic characteristics of the test building and its nonstructural components and systems. All earthquake and WN motions were applied in the east-west direction using the single-axis shake table, whose axis coincided with the longitudinal axis of the building. The earthquake input motions and measured building peak responses are summarized in Table I. This table summarizes the PFAs at the roof and the PIDRs at level 2,
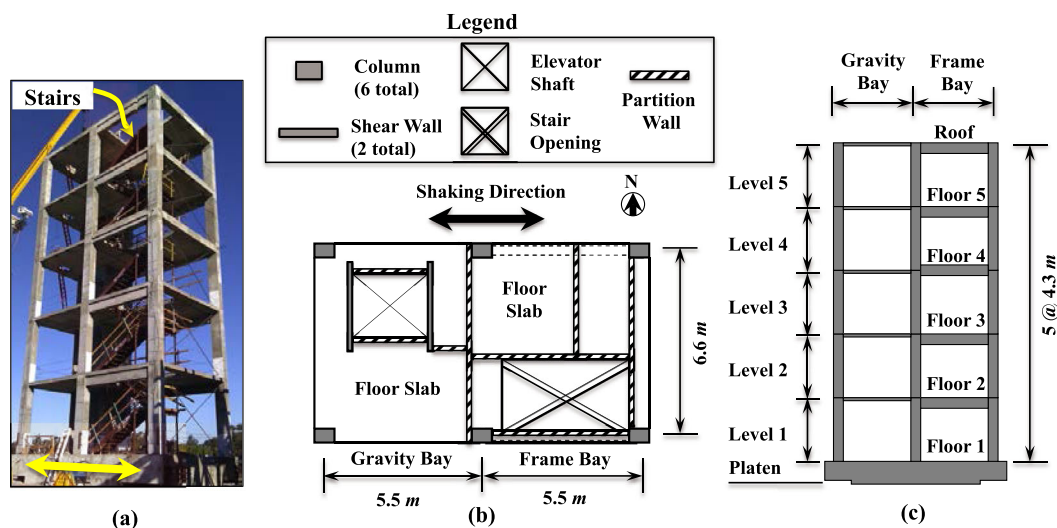

Figure 2. Test building: (a) photograph of structural skeleton, (b) schematics of plan layout (level 3), and (c) schematics of elevation (shear walls not shown).

Table I. Summary of earthquake input motions and measured building peak responses.

Test phase	Motion name	Earthquake input motions					Building responses	
		PIA^1 (g)	PIV^2 (m/s)	PID^3 (m)	$S_a(T_1,\xi)^4$ (g)	$T_d{}^5$ (s)	$PFA_R{}^6$ (g)	$PIDR_{L2}{}^7$ (%)
Base isolated (BI)	BI-1:CNP100	0.21	0.23	0.08	0.09	15	0.09	0.08
	BI-2:LAC100	0.22	0.24	0.09	0.06	20	0.10	0.10
	BI-3:LAC100	0.25	0.24	0.09	0.08	20	0.10	0.11
	BI-4:SP100	0.52	0.35	0.08	0.08	80	0.12	0.10
	BI-5:ICA50	0.17	0.22	0.04	0.08	130	0.08	0.09
	BI-6:ICA100	0.31	0.43	0.09	0.15	128	0.16	0.19
	BI-7:ICA140	0.50	0.63	0.13	0.23	97	0.26	0.32
Fixed base (FB)	FB-1:CNP100	0.21	0.24	0.09	0.33	15	0.44	0.47
	FB-2:LAC100	0.18	0.23	0.09	0.29	20	0.39	0.56
	FB-3:ICA50	0.21	0.26	0.06	0.47	91	0.58	0.94
	FB-4:ICA100	0.26	0.28	0.07	0.46	96	0.64	1.41
	FB-5:DEN67	0.64	0.64	0.20	1.13	49	0.99	2.75
	FB-6:DEN100	0.80	0.84	0.34	1.36	49	0.90	5.99

[1] PIA – (achieved) peak input acceleration;
[2] PIV – (achieved) peak input velocity;
[3] PID – (achieved) peak input displacement;
[4] $S_a(T_1,\xi)$ – elastic spectral acceleration of the input motion ($T_1 = 2.5\ s$ and $\xi = 12\%$ for the BI test, $T_1 = 1.0\ s$ and $\xi = 5\%$ for the FB tests);
[5] T_d – strong motion duration (defined as the time interval between 5% and 95% total Arias intensity of the input motion);
[6] PFA_R – (averaged) peak floor acceleration measured at the roof;
[7] $PIDR_{L2}$ – (averaged) peak interstory drift ratio measured at level 2.

which represent the largest peak responses of the test building during each test. It is also noted that although the building fundamental period T_1 varied during the testing because of accumulated structural damage, reference values of 2.5 s for the building in the base-isolated test phase and 1.0 s for the fixed-base test phase are used for evaluating the elastic spectral accelerations at the building fundamental period $S_a(T_1,\xi)$. The damping ratio $\xi = 12\%$ is selected for the base-isolated tests, which provides reasonable estimates of the measured peak roof accelerations using an equivalent linear single-degree-of-freedom system with this damping ratio, while a value of $\xi = 5\%$ is used for the fixed-based tests.

As the seismic demands on the building (superstructure) were relatively low (with PIDR < 0.4% and PFA < 0.3 g) in the BI test phase, the building sustained only minor damage to its most brittle non-structural components (e.g., partition walls [15]) and very little damage to its structural components. In the FB test phase, the earthquake motions were applied with increasing intensity to progressively damage the structure. The building was severely damaged during the last two FB tests. Physical damage during test FB-6 included fracture of the longitudinal reinforcement at the ends of the frame beams and punching shear mechanisms at the slab–column interfaces of the second and third floors. This resulted in the development of a soft story mechanism at the lower levels of the test building (also known as an intermediate failure mechanism) [16, 17]. It is notable that the design target PIDR of about 2.5% was achieved during test FB-5, while well above the design target PIDR of 6% was attained during test FB-6. Interested readers may find additional information regarding the broader test program and results in [12–14].

3. PREFABRICATED STEEL STAIRS

The prefabricated steel stairs were located on the southeast side of the building (Figure 2(b)) and provided access to all floors including the roof. As shown in Figure 3, the stair assembly at each level was installed in a scissor configuration, consisting of a mid-level landing and two parallel straight flights running in opposite directions from the landing. The flights, landings, and handrails were factory
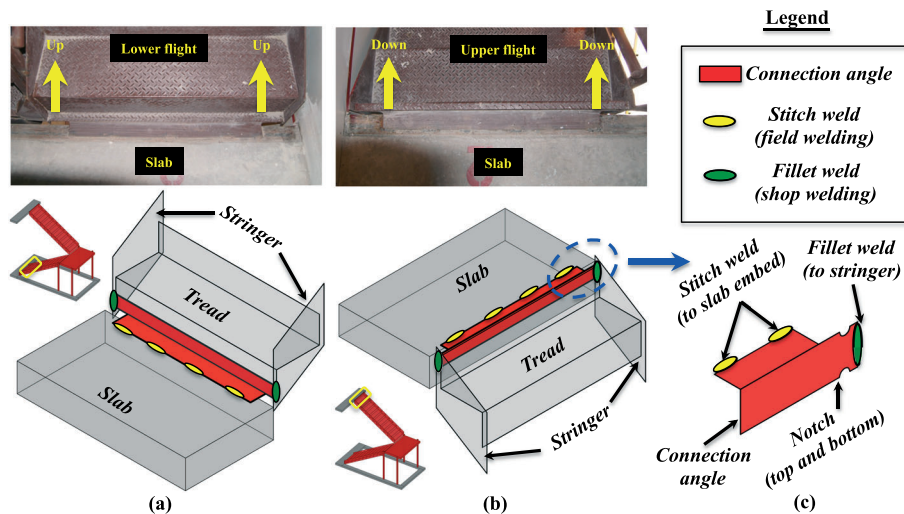
Figure 3. Stair layout: (a) three-dimensional schematic of the stair (handrail not shown for clarity), (b) photograph of the stair installed in place during structural skeleton completion, and (c) photograph of the stairwell at building completion. Note that double-headed arrow denotes the direction of input motion applied at the base of the test building.

fabricated and installed in place by the stair manufacturer in conjunction with construction of the building. The in-place installation consisted of welding of the flights and landing posts to steel embeds cast within the beams and slabs of the test building. Bolted connections were only utilized at connections between the flights and the landings. The total weight of the stair was approximately 10.1 kN, with 3.3 kN from the landing and 3.4 kN from each of the flights (including handrails). The stairs were enclosed within cold-formed steel framed gypsum partition walls framed from floor to floor on all sides of the openings (Figure 2(b) and 3(c)). A nominal gap between the stairs and the partition wall enclosure was provided and ranged between 30 and 40 mm.

3.1. Specimen description

3.1.1. Flights and landing. The flight stringers utilized ASTM A36 25.4-mm thick plates, and the treads and risers were constructed with 14 gage checkered plates welded to the stringers. Each flight consisted of 11 steps, with a horizontal projected length of 3.07 m and a vertical projected height of

Figure 4. Flight-to-building connection details: (a) lower flight to slab connection, (b) upper flight to slab connection, and (c) upper flight connection angle.

2.13 m. The 1.07 × 2.24 m landing deck was supported on two ASTM A36 C200 × 17.1 joists placed in the transverse-to-stair-run direction. Four ASTM A36 76.2 × 76.2 × 6.4 mm hollow structural section (HSS) landing posts provided vertical support to the landing joists at the corners at each level. These landing posts were each connected to the landing joists using two 16-mm diameter ASTM A325 bolts and were fillet welded to steel embeds cast with the building at their base. In addition, the connections between the (upper and lower) flights and the landing joists utilized two 16-mm diameter ASTM A325 tension control bolts per flight.

3.1.2. Flight-to-building connections. With the exception of the lower flight at level 1, which was connected to the slab at the first floor (foundation) using post-installed wedge anchors, the lower flights at level 2 through level 5 were each connected to the building using an ASTM A36 L102 ×76× 6.4 mm angle (Figure 4(a)). Likewise, the upper flights at all levels were each connected to the building using an ASTM A36 L76 × 51× 6.4 mm angle (Figure 4(b)). All these connection angles were shop welded to the stair stringers at each end and field welded to the steel embed cast with the building using 51 mm long stitch welds spaced at 305 mm on center. It is noteworthy that while the lower flight to building connections were designed to provide limited deformability, the upper flight connection angles differed from those at the lower flight because of the presence of a pair of notches at the ends of the vertical legs of the connection angles (Figure 4(c)). These notches were intended to facilitate floor-to-floor relative motions and intended to yield during design interstory drift demands.

3.2. Instrumentation

The stairs were instrumented with an array of 20 uni-axial accelerometers and 30 displacement transducers, accounting for about 10% of the total sensors deployed within the test specimen. These sensors were connected to a multi-node distributed data acquisition system, which collected data simultaneously at a sampling frequency of 240 Hz. It is noted that while the accelerometers on the stairs were all installed prior to the tests, the displacement transducers were modified as needed during the test program. Figure 5 presents the instrumentation of the stair at level 2 during test FB-6. It is noted that each sensor channel is assigned with a unique name, and these names are used in the discussion of the measured stair response later in this paper. As shown in the figure, the stair at level 2 was densely instrumented and included eighteen accelerometers, six each on the flights and the landing, and eight displacement transducers (D-L-1 through D-L-8) measuring relative deformations of the stair connections as well as three between the landing and surrounding partition walls (D-L-9, D-L-10, and D-T-1). Four networked video cameras were also deployed at the stairwell to monitor the physical behavior of
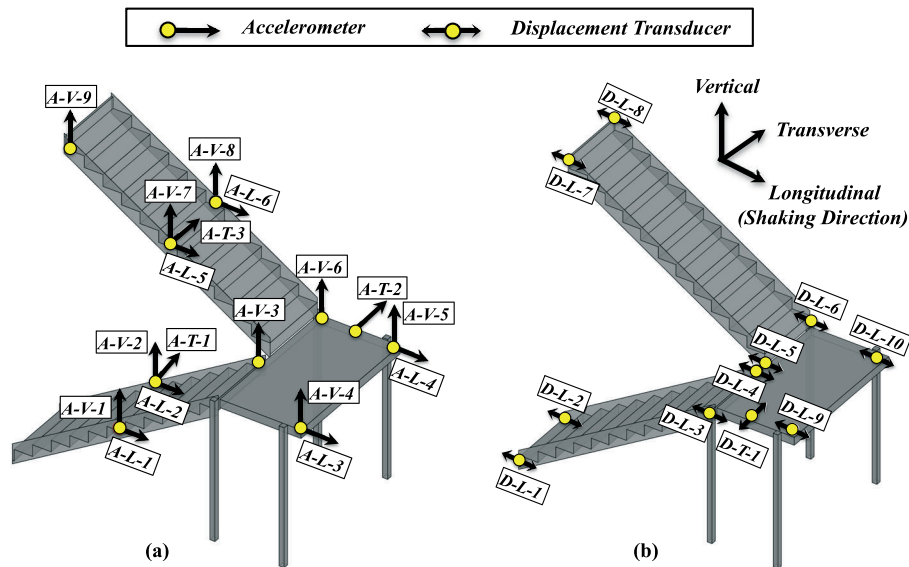
Figure 5. Instrumentation of the stair at level 2: (a) accelerometers and (b) displacement transducers. Sensor orientations shown are consistent with the global coordinate system used for the building. Note that level 2 as the most densely instrumented level of stairs.

the stairs. The response of the building structure was measured with a dense accelerometer array consisting of four tri-axial accelerometers installed at the corners of each floor of the building. It is noted, however, that these tri-axial accelerometers were connected to a stand-alone data acquisition system sampling data at a frequency of 200 Hz. Additional details of the instrumentation of the stairs and the test building can be found in [18].

4. SYSTEM IDENTIFICATION OF STAIRS

Low-amplitude WN base excitations were applied to the building using the shake table at various stages during the test program. Although low amplitude, the modal parameters derived from these tests provide a unique understanding of the initial dynamic characteristics of the stairs and are useful for numerical model calibration. Using measurements from these WN tests, the deterministic-stochastic identification (DSI) method [19] is used to estimate the modal parameters (natural frequencies, damping ratios, and mode shapes) of the stairs. The DSI method is a time-domain system identification method that realizes a linear state-space model using input–output data. It is robust to both process noise and measurement noise because both terms are explicitly considered in its formulation. Furthermore, it is suitable for dynamic systems with multiple inputs (multiple-support excitations). This method has been applied successfully to identify the modal parameters of the full-scale test building [20] as well as other large-scale structures in previous shake table tests [21, 22]. However, unlike the building that considered base excitation as the single input for the system, the system identification of stairs requires consideration of multiple inputs because the stairs were subjected to excitations from both the upper and lower floors of the building in the WN tests.

The system identification focuses on the stair at level 2, because it represented the most densely instrumented stair in the test building. As shown in Table II, four WN tests are selected for system identification of the stair, each associated with a representative state during the test program. Tests S0 and S2 correspond to the beginning and end states of the base-isolated test phase, respectively, while test S1 corresponds to an intermediate state during this test phase. Test S3 corresponds to the beginning state of the fixed-base test phase. It is noted that test S3 is the only WN test in the fixed-base test phase prior to the occurrence of severe damage of the stair at level 2. All subsequent WN tests in the fixed-base test phase were conducted after test FB-4. As the stair sustained severe damage during test FB-4 and the subsequent two fixed-base earthquake tests, this rendered the system identification results unstable.

Table II. White noise base excitation tests selected for stair system identification.

State	Test configuration	$PIDR_{L2}$[1] (%)	Cumulative number of interstory drift ratio cycle
S0 (before BI-1)	BI	N/A	0
S1 (after BI-5)	BI	0.11	29
S2 (after BI-7)	BI	0.32	83
S3 (before FB-1)	FB	0.32	83

[1] Peak interstory drift achieved at level 2.

Each of the selected WN tests consisted of input excitations of three distinct amplitude levels with root-mean-square (RMS) accelerations of 1.5% g, 3.0% g, and 3.5% g . For result comparison purposes, the state of the stair during the 1.5% g RMS WN test S0 (at the beginning of the test program) is selected as the reference state. Table II also summarizes the PIDR and the cumulative number of interstory drift ratio (IDR) cycles of level 2 of the test building corresponding to each representative state. It is noted that both the PIDR and the IDR cycles consider the interstory drift response from the beginning of the test program to the beginning of each WN test. The cumulative number of IDR cycles are determined using the rainflow counting method [23], in which the IDR bins are centered at values starting from 0.1% to the maximum IDR at a constant width of 0.1% (e.g., the first bin represents a range between 0.05% and 0.15%). It is also noted that IDR cycles with amplitudes less than 0.05% are excluded from the cycle-counting algorithm, as their effects on the damage to the stairs are considered insignificant. Provided the fact that the interstory drifts of the building were insignificantly small (<0.05%) during the WN tests in the base-isolated test phase, the cumulative IDR cycles as presented in Table II are the contributions of the seismic tests. This also explains the fact that the PIDR and the cumulative IDR cycles remained unchanged from state S2 to S3, because no seismic test was conducted between these two states.

In the system identification procedure, the averaged absolute longitudinal accelerations measured on the second and third floors of the building are used as input data, while the accelerations measured on the stair at level 2 are used as output data. To illustrate the characteristics of the input and output data of the system, Figure 6 presents the acceleration responses measured on the second floor of the building and the stair at level 2 during the reference state (1.5% g RMS WN test S0). Because the base excitation applied to the building was only in the longitudinal direction, the amplitudes of the transverse floor accelerations were much smaller than (about 5%) their longitudinal counterparts in the WN tests (Figure 6(a)). In addition, the longitudinal floor accelerations measured at the four corners of the building were very similar to each other, as the relative RMS errors between the floor accelerations at the corners and the averaged floor accelerations were generally less than 5%. In this regard, only the averaged longitudinal accelerations at the lower (second) and upper (third) floors are considered as input data for the stair at level 2. Despite the predominant longitudinal floor excitations, the stair landing and flights observed acceleration responses of comparable amplitudes in all three directions (Figure 6(b)). In addition, the frequency contents of these acceleration responses differed considerably. The spectral peaks as observed in the frequency range different from those of the building (5–25 Hz) are indications of modal frequencies of the stair. Therefore, the output data considers the stair accelerations measured in all three directions. This results in a multiple-input multiple-output system with two input and eighteen output channels. It is noted that the input and output data were filtered with a fourth-order Butterworth filter using band-pass frequency between 0.25 and 50 Hz. In addition, the input and output data were recorded using separate data acquisition systems sampling data at different frequencies (i.e., 200 Hz for the building and 240 Hz for the stairs), and therefore, the measured accelerations were resampled and synchronized before applying the system identification algorithm. The processed data were resampled to 100 Hz such that the Nyquist frequency (50 Hz) is much higher than the modal frequencies of interest in this study.

Stability diagrams, which are not shown for brevity, indicate that three stable vibration modes are consistently present in the WN tests. Figure 7 presents the polar plot representations of the complex-valued mode shapes identified at the reference state (1.5% g RMS WN test S0). It is observed that the three identified modes are nearly classically damped because the mode shape components are nearly
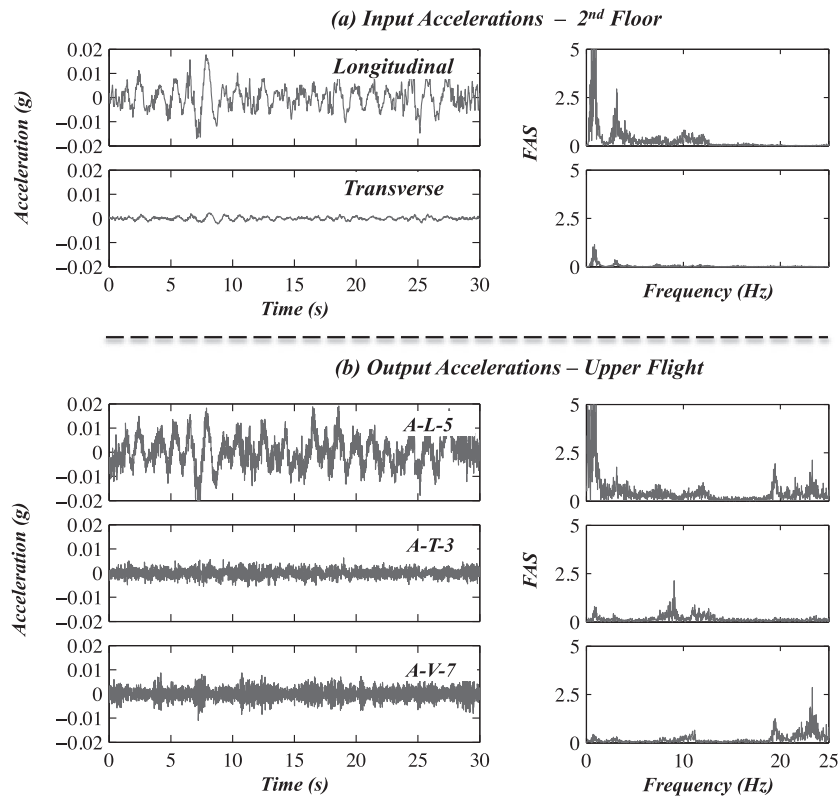
Figure 6. Selected (a) input and (b) output acceleration histories and corresponding Fourier amplitude spectra during the reference state (1.5% g root-mean-square white noise test S0).
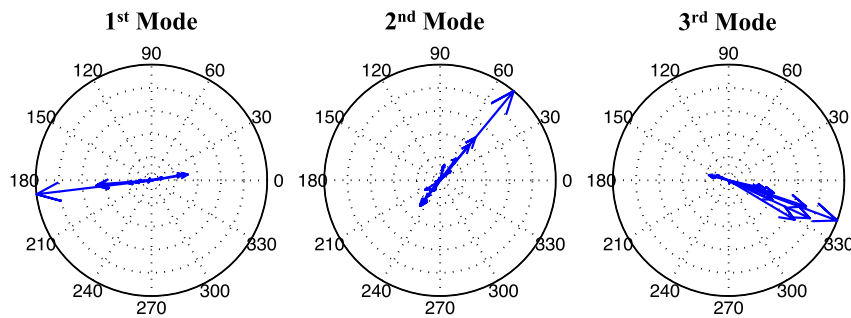

Figure 7. Polar plot representations of the complex-valued mode shapes identified at the reference state (1.5% g root-mean-square white noise test S0).

collinear. The real-valued mode shapes of the stair obtained using the method proposed by Imregun and Ewins [24] are shown in Figure 8. The first and second modes both correspond to global torsional vibration modes of the stair and the third mode represents global vibration of the stair in its parallel-to-flight direction. Importantly, each of the three identified modes includes vertical vibration of the flights. It is noted that the first and second modes exhibit very similar mode shapes. This is because the effects of the handrails are not considered in the identification in the absence of measurements on the handrails, while they accounted for about 30% of the total mass of the stair at each level. This is confirmed by eigen-value analysis results using a finite element model of the stair, which indicates that the deformation of the handrails differs completely in these two modes, even though the deformation of the flights and landing appears similar [25].

Table III summarizes the identified natural frequencies, damping ratios, and modal assurance criterion (MAC) values [26] for the three identified modes at different WN test states. The MAC values
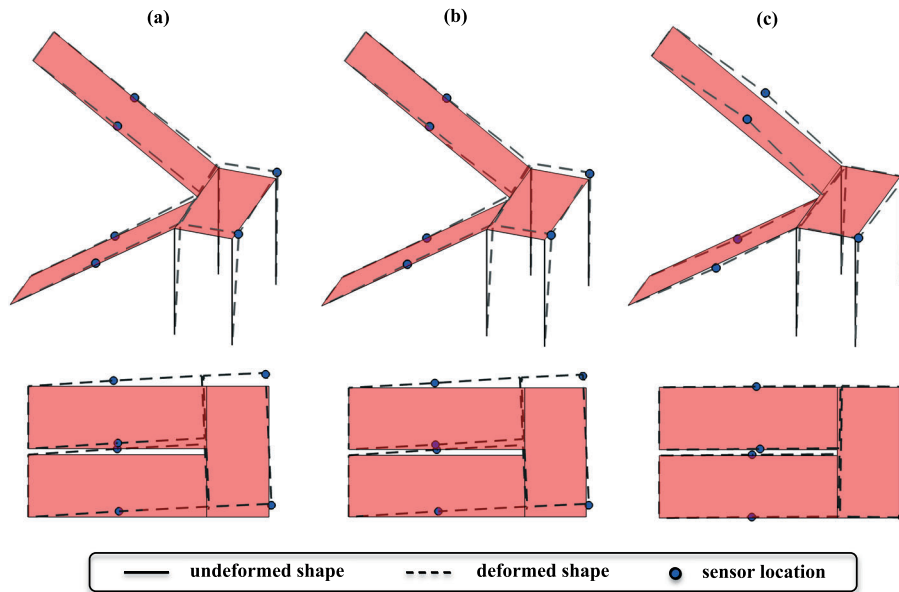
Figure 8. Identified mode shapes: (a) first mode, (b) second mode, and (c) third mode.

Table III. Identified modal parameters of the stair at different white noise (WN) test states.

WN test		1st mode			2nd mode			3rd mode		
State	RMS[2] Amp.	Frequency[1] (Hz)	ξ (%)	MAC[3]	Frequency[1] (Hz)	ξ (%)	MAC	Frequency[1] (Hz)	ξ (%)	MAC
S0	1.5% g	8.88 [100]	4.17	1.00	11.14 [100]	4.52	1.00	19.75 [100]	1.01	1.00
	3.0% g	8.78 [98.9]	4.21	1.00	11.20 [100.5]	4.01	0.99	19.50 [98.7]	1.26	0.99
	3.5% g	8.76 [98.6]	4.10	0.99	11.10 [99.6]	3.68	0.99	19.47 [98.6]	0.72	0.99
S1	1.5% g	8.90 [100.2]	4.17	1.00	11.16 [100.2]	4.62	1.00	19.74 [99.9]	1.03	1.00
	3.0% g	8.79 [99.0]	4.21	0.99	11.21 [100.6]	4.07	0.98	19.51 [98.8]	1.27	0.99
	3.5% g	8.78 [98.9]	4.13	0.99	11.14 [100]	3.68	0.99	19.44 [98.4]	0.72	0.99
S2	1.5% g	8.53 [96.1]	5.64	0.99	11.07 [99.4]	2.32	0.96	19.02 [96.3]	1.46	0.97
	3.0% g	8.52 [95.9]	4.51	0.99	11.10 [99.6]	2.72	0.94	18.91 [95.7]	1.42	0.98
	3.5% g	8.50 [95.7]	4.71	0.98	11.03 [99.0]	2.83	0.94	18.85 [95.4]	1.29	0.94
S3	1.5% g	8.37 [94.2]	3.95	0.99	11.02 [98.9]	1.32	0.95	18.74 [94.9]	1.21	0.95
	3.0% g	8.29 [93.4]	4.85	0.99	10.90 [97.8]	2.68	0.93	18.57 [94.0]	1.63	0.94
	3.5% g	8.22 [92.6]	4.39	0.99	10.76 [96.6]	3.01	0.92	18.31 [92.7]	2.12	0.94

[1] Value in the square bracket shows the frequency relative to that in the reference state (1.5% g RMS WN test S0), unit in percentage; [2] root-mean-square amplitude of the white noise excitation; MAC[3], modal assurance criterion.

are computed between each identified mode shape and its counterpart identified at the reference state (1.5% g RMS WN test S0). Important observations from the modal identification results are as follows:

(1) The identified natural frequencies at state S1 remained nearly identical with those at state S0, as the building experienced very low PIDR demands (0.11%) prior to state S1 and accumulated IDR cycles (29). However, the natural frequencies slightly decreased in state S2 as the PIDR (0.32%) and the cumulative number of IDR cycles (83) increased. Although the PIDR and cumulative number of IDR cycles remained unchanged between state S2 and S3, the natural frequencies underwent further decrease at state S3. This is due to the larger amplitude of the interstory drifts during the WN test S3, because the building was fixed at its base at state S3. These observations suggest that the accumulation of IDR cycles as well as larger PIDR result in reduction of the identified natural frequencies for the system.

(2) The identified damping ratios are primarily in the range of 1–5% during these WN tests. The first two modes (torsional) present notably higher values of damping ratio than those of the third mode (longitudinal) in the reference state (1.5% g RMS WN test S0). In most cases, the identified damping ratios of the third mode slightly increased, and the values of the first two modes decreased as IDR cycles accumulated. However, unlike the case of natural frequencies, the damping ratios do not consistently correlate with the increase of PIDR or the accumulation of IDR cycles.

(3) The MAC values for the three identified modes are reasonably close to unity in the first two states (S0 and S1). During the last two states (S2 and S3), the calculated MAC values of the higher modes slightly deviate from unity as a result of the accumulated IDR cycles and the increased PIDR. However, all identified MAC values remain larger than 0.9, indicating that the identified mode shapes are consistent with those at the respective identified reference states (1.5% g RMS WN test S0).

(4) The experimentally identified modal parameters (e.g., frequency, damping ratio, and mode shape) can be used for verification of numerical models of the stairs and therefore improving the predictive capacity of such models when used in time history analysis. However, it is noteworthy that the parameters identified using the DSI system identification method are developed based on linear system theory, and, therefore, the identified results represent those of an equivalent linear system at their specific states. The dynamic response of the stairs is nonlinear from the onset of loading even when subjected to low-amplitude excitations. The physical dissipative sources of nonlinearity (e.g., friction, yielding, and contact) are lumped into the identified equivalent viscous damping. Therefore, direct application of the identified damping ratios in structural modeling for nonlinear time history analysis may lead to erroneous results.

5. SEISMIC TEST RESULTS

5.1. Physical observations

5.1.1. Damage metrics and repair actions. Post-shaking inspection of the stairs were conducted at each inspection phase to characterize their physical damage. Damage documentation relied upon visual inspections as well as detailed photographs, videos, and notes. It is noted that inspections of the weld connections at the bottom of the landing posts were not possible because they were enclosed within
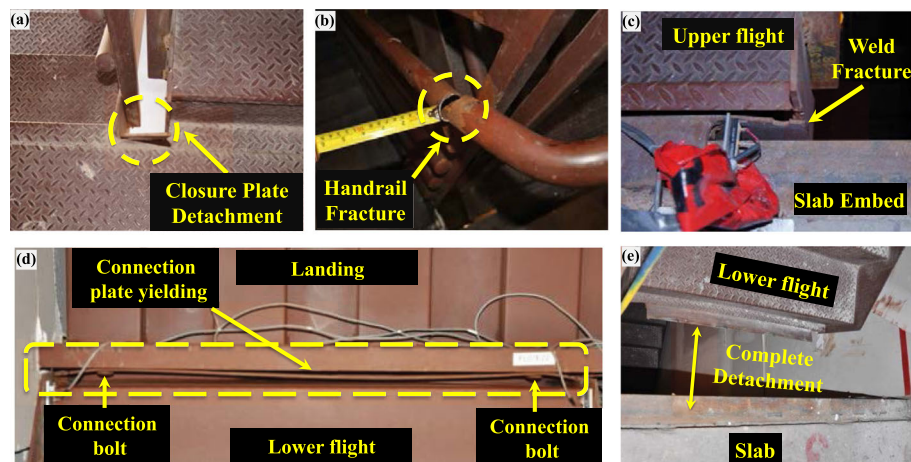

Figure 9. Examples of observed stair damage: (a) closure plate detachment (DS-1; photograph taken at the landing between level 1 and 2 after test FB-4), (b) handrail fracture (DS-1; photograph taken at level 3 after test FB-5), (c) upper flight connection angle weld fracture (DS-3; photograph taken at level 3 following test FB-4), (d) plastic yielding of the connection plate between the landing and lower flight (DS-2; photograph showing the bottom view of the landing at level 2 following test FB-5), and (e) lower flight detachment and complete loss of vertical support (DS-3; photograph taken at level 3 after test FB-6).

Table IV.   Stair damage states and physical descriptions of the damage mechanisms.

Damage state	Damage implications and corresponding repair actions	Physical descriptions of the damage mechanisms
DS-1 (minor)	No immediate repair needed for continued service	Closure plate detachment (Figure 9(a)); handrail fracture (Figure 9(b))
DS-2 (moderate)	Repair needed with minimal disruption to service, safe egress prior to repair is possible by occupants	Connection plate yielding (Figure 9(d)); anchor bolt washer plate yielding
DS-3 (severe)	Immediate repair needed with downtime required to assure service (this state may be unsafe for egress)	Connection weld fracture (Figure 9(c)); flight detachment (Figure 9(e))
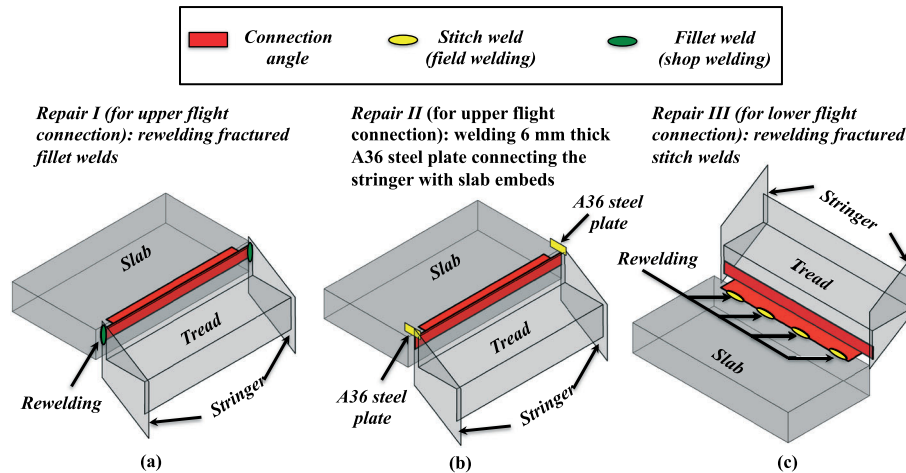
Figure 10.   Stair repair actions: (a) R-I, (b) R-II, and (c) R-III (only the welds that require repair are shown in the figure).

the partition walls. As shown in Figure 9, five common types of damage mechanisms were observed during the tests. These are categorized into three distinct damage states (DSs) according to their implications on stair functionality and repair actions. The definitions of the damage states and the physical description of the observed damage are summarized in Table IV, and the repair actions implemented in these tests for the different damage mechanisms are illustrated in Figure 10. It is noted that, while no repair action was taken for minor and moderate damage during these tests, severe damage to the stairs was repaired immediately to restore safe access to the test building and to allow the execution of subsequent tests.

5.1.2. Damage progression. No physical damage to the stairs was observed in the BI test phase and the first three FB tests, as the building drift demands remained relatively low (PIDR < 1%). Damage to the stairs initiated during test FB-4 and became extensive in the last two FB tests. Figure 11 illustrates the progression of stair damage as observed post-shake at each of the last three FB tests and the associated repair actions. The associated PIDRs during the specified seismic tests (as boxed and in black) and the IDRs related to the exact time of damage occurrence (in parenthesis and in red when available) are also presented in this figure. *FB-4:ICA100* – Inspection following test FB-4 indicated a detached closure plate (DS-1) at the landing at level 1 (Figure 9(a)) as well as fracture of the upper flight connection angle vertical fillet welds (DS-3) at levels 2 (Figure 9(c)) and 4. It is noted that although complete detachment and subsequent loss of vertical support did not occur, the service capacity of the stair was compromised, as its lateral connectivity to the building was non-existent at these two levels. The two cases of weld fracture were repaired prior to test FB-5 as follows: (i) re-welding of the upper flight connection angle to the stringer (R-I) at level 4 (Figure 10(a)) and (ii) welding steel plates between the upper flight stringer and the slab embed (R-II) at level 2 (Figure 10(b)).
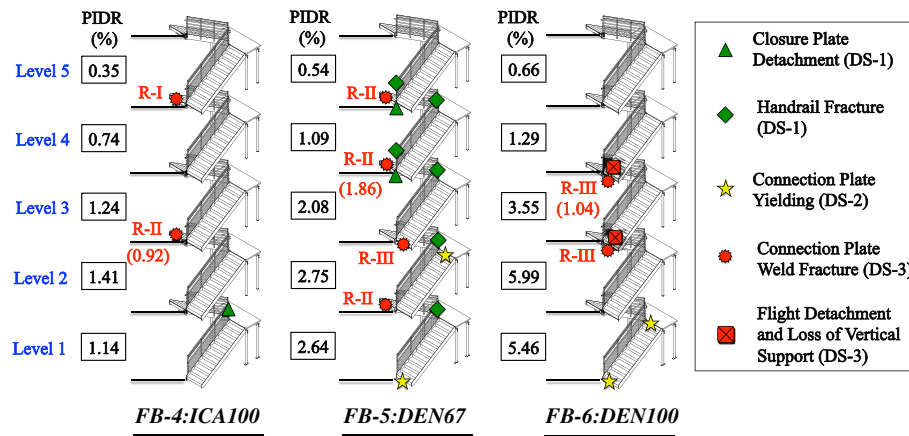
Figure 11. Stair damage progression during the last three fixed-base (FB) tests (notes: damage types are differentiated by color and marker shape, that is, red for DS-3, yellow for DS-2, and green for DS-1; boxed values represent peak interstory drift ratios (PIDRs) during the specified seismic tests and are shown in black, and red values in parenthesis represent the actual interstory drift ratios (IDRs) at damage instance).

FB-5:DEN67 – Damage to the stairs was distributed at various locations in the form of closure plate detachment (DS-1), handrail fracture (DS-1) (Figure 9(b)), connection plate yielding (DS-2) (Figure 9(d)), and connection weld fracture (DS-3). Severe damage that required immediate repair included (i) the lower flight connection angle stitch weld fracture (note that the lower flight did not slide off of its vertical support at the slab embeds, however it was completely detached) at level 3 (DS-3) and (ii) the upper flight connection angle vertical fillet weld fractures (DS-3) at levels 1, 3, and 4. Repair of the lower flight connection angle stitch weld fracture was conducted by re-welding of the lower flight connection angle to the slab embed (R-III), and the three cases of the upper flight connection angle vertical weld fracture were repaired by R-II. In addition, plastic yielding occurred at the connection plate (DS-2) between the landing and the lower flight at level 2 as well as at the washer plates (DS-2) of the lower flight to landing connection at level 1.

FB-6:DEN100 – The lower flights at levels 3 and 4 completely detached and slid off of their vertical support at the slab embeds (DS-3) because of complete weld failure (Figure 9(e)). Repair of the detached flights involved use of a pulley to re-position the flights in place and subsequent re-welding of the flights to the slab embeds (R-III). In addition, plastic yielding of the connection plate (DS-2) between the landing and the lower flight at level 1 was detected, and the washer plates of the lower flight to landing connection at level 1 suffered continued plastic deformation (DS-2).

Physical inspection during building demolition revealed complete fracture of the welds between the landing posts and the slab embeds at the lower three levels. This type of damage rendered the landings unattached at their base. However, the onset of these weld fractures is uncertain, because these connections were enclosed within the partition walls during the seismic tests.

Summary of Physical Damage – These physical damage observations highlight that stair damage was sensitive to interstory drift demands of the building. It is noted that test FB-5 represents an earthquake scenario that achieved the design performance objectives of the building (PIDR of 2.5%), and that this design target PIDR is comparable with prescribed values in ASCE 7-10 [6]. This test (FB-5) coincidentally also caused four instances of severe damage to the stairs, including at levels of PIDR below the 2.5% performance target.

During all seismic tests, eight instances of severe damage were detected at all levels except at level 5. Severe damage to the stairs at each level initiated consistently in the form of upper flight connection angle vertical fillet weld fracture, with associated PIDRs of 2.64% at level 1 (test FB-5), 1.41 at level 2 (test FB-4), 2.08 at level 3 (test FB-5), and 0.74 at level 4 (test FB-4). Notably, even prior to attainment of the building design target PIDR, safe egress from the building was compromised during test FB-4 as a result of the two occurrences of upper flight connection angle vertical fillet weld fracture. The associated PIDRs, which caused this severe damage (0.74% and 1.41%), were much lower than the design performance target (PIDR of 2.5%). During the last two FB tests, severe damage to the

stairs continued to occur in the form of upper flight connection angle vertical fillet weld fracture, lower flight connection angle stitch weld fracture, and ultimately complete lower flight detachment that rendered the stairs completely inoperable. It is noteworthy that ground motions as intense as those of the last two fixed-base tests can result in the development of a double-story mechanism, also known as an intermediate failure mechanism [16, 17], in reinforced concrete moment resisting frames designed according to the ACI 318 code [27]. This aspect further complicates the seismic design of stairs because large drift demands tend to concentrate at only a few levels of a special moment frame building.

5.1.3. Identification of time instance of damage occurrence. The PIDR represents the absolute maximum of an interstory drift history and may not coincide with the IDR at which the most pronounced damage occurs. Fortunately, during these tests, additional time-synchronized measurement sources were available at select locations to allow identification of time instances of the stair damage. Table V summarizes two instances of upper flight connection angle vertical weld fracture, which were identified using the data measured by the displacement transducers and the video camera monitoring the stair connections. These two damage instances both corresponded to the initial damage occurrences at the individual locations. The IDR cycles are also determined using the rainflow counting method [23] (similar to the procedure used in Table II). These cycles account for the contribution of both the seismic tests and the low-amplitude WN base excitation tests from the beginning of the test program until the occurrence of the damage. Figure 12 provides the distributions of the IDR cycles as well as the associated IDR time histories corresponding to the two damage instances. IDR cycles less than 0.05% are excluded from the cycle counting, because these cycles are considered insignificant to affect the

Table V. Damage instances for the two upper flight connection angle vertical weld fracture failures (DS-3).

			$PIDR^2$ (%)	IDR^3_{damage} (%)	IDR^4 Cycles	
Test	Location	Data source[1]	[time (sec)]	[time (sec)]	Total	High-amplitude
FB-4	Level 2	displacement sensor	1.41 [29.34]	0.92 [27.56]	668	33.5
FB-5	Level 3	video camera	2.08 [46.42]	1.86 [38.72]	960	66.0

[1]Data source refers to the measurement source to obtain the IDR_{damage}; 2 peak interstory drift ratio; 3 the time instantce of stiar damage; 4 interstory drift ratio.
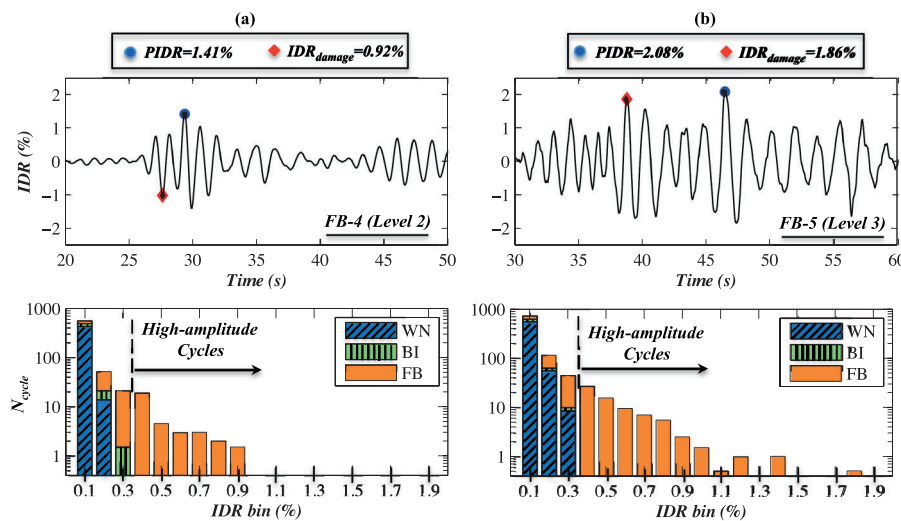

Figure 12. Interstory drift response and the accumulated interstory drift ratio (IDR) cycle distribution for the two instances of upper flight connection angle vertical weld fracture: (a) FB:4-ICA100 and (b) FB-5:DEN67. (PIDR), peak interstory drift ratio; (WN), white noise tests; (BI), base-isolated seismic tests; (FB), fixed-base seismic tests.
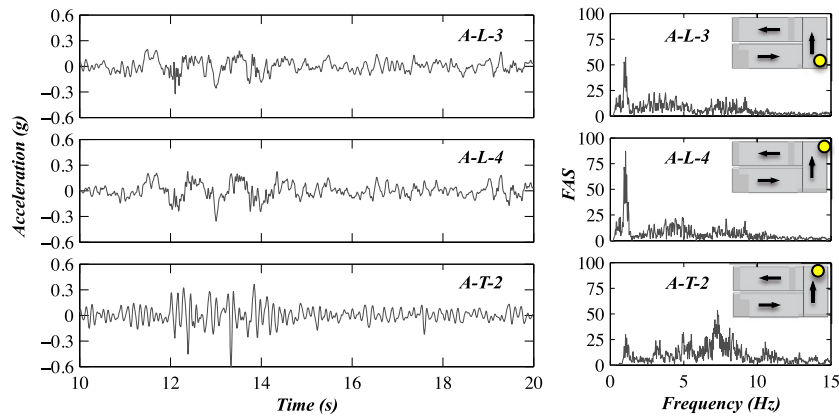
Figure 13. Absolute acceleration time histories and corresponding Fourier amplitude spectra (FAS) of the stair landing at level 2 during test FB-1.

stair responses, while cycles in the 0.4% or larger IDR bins are defined as high-amplitude IDR cycles as numerical simulation of the stairs suggests that plastic yielding of the upper flight connection plate occurs at an IDR lower than 0.4% [25].

As shown in Figure 12, the majority of low-amplitude cycles (0.1–0.3% bins) occurred during the WN and base-isolated tests, while high-amplitude cycles (0.4%-and-higher bins) were exclusively attributed to the fixed-base tests. It is also shown in Figure 12 that the stair at level 3 experienced 66 high-amplitude IDR cycles prior to the weld fracture, as compared with 33.5 cycles for the same type of damage, which occurred at level 2. The two damage instances may not provide adequate information on the low-cycle fatigue behavior of the welds; however, these observations do not warrant a clear trend of loading histories on the weld fracture, because the stair that was damaged at a higher IDR value (1.86%) underwent twice as many high-amplitude cycles as the one damaged at a lower IDR value (0.92%).

5.2. Measured responses

5.2.1. Acceleration response. The absolute acceleration time histories of the stair landing at level 2 during test FB-1 and the corresponding Fourier amplitude spectra (FAS) are presented in Figure 13. The measured acceleration responses were filtered with a fourth-order Butterworth filter with band-pass frequencies between 0.25 and 25 Hz. The longitudinal accelerations at the two corners of the stair landing (A-L-3 and A-L-4, Figure 5(a)) were comparable, and their amplitudes were both similar to those at the upper and lower floors [14]. Despite the insignificantly small floor excitations in the transverse direction, the amplitude of the transverse landing acceleration (A-T-2) is even larger than its longitudinal counterparts (A-L-3 and A-L-4). In addition, it is observed that the FAS peak of the landing longitudinal acceleration responses occur at around 1 Hz, which correspond to the first longitudinal vibration mode of the building at this damage state, while the landing transverse acceleration response was predominately attributed to the first torsional vibration mode of the stair at a higher frequency around 7.5 Hz. This frequency also corresponds to the higher modes of the building in its fixed-base configuration [20].

Table VI summarizes the peak component accelerations (PCAs) of the stair landing at level 2 and the PFAs at the corresponding floors for all base-isolated and the first three fixed-base seismic tests. In this case, the PCA is defined as the absolute maximum of the landing acceleration time history. It is noted, however, that the landing observed frequent high-frequency acceleration spikes during the last three FB tests as a result of pounding of the stair with its surrounding partition walls as well as abrupt connection weld fractures. These high-frequency responses are not representative of the dynamic characteristics of the stairs and are instead a result of the practical configuration of the stairs with their adjacent systems. As a result, these values are excluded from the table. During the base-isolated tests, the acceleration response of the landing underwent no amplification in the longitudinal direction, as the ratios between

Table VI. Peak acceleration responses of the stair landing at level 2.

| Test name | PFA | | $PCA_{long}^{landing}$ | $PCA_{trans}^{landing}$ | $\dfrac{PCA_{long}^{landing}}{PFA_{ave}}$ | $\dfrac{PCA_{trans}^{landing}}{PCA_{long}^{landing}}$ |
	2nd floor (g)	3rd floor (g)	(g)	(g)	(%)	(%)
BI-1:CNP100	0.08	0.07	0.07	0.02	92	35
BI-2:LAC100	0.09	0.08	0.08	0.03	88	39
BI-3:LAC100	0.09	0.08	0.08	0.03	89	42
BI-4:SP100	0.08	0.09	0.09	0.04	99	42
BI-5:ICA50	0.07	0.08	0.08	0.02	98	22
BI-6:ICA100	0.14	0.14	0.14	0.03	97	22
BI-7:ICA140	0.20	0.21	0.20	0.08	97	41
FB-1:CNP100	0.27	0.32	0.36	0.59	115	179
FB-2:LAC100	0.28	0.31	0.28	0.44	98	164
FB-3:ICA50	0.24	0.35	0.40	0.53	131	138

Notes: PFA – peak floor acceleration; PFA_{ave} – peak floor acceleration as averaged between the floors above and below the landings of level 2; $PCA_{long}^{landing}$ – peak component acceleration of the stair landing in the longitudinal direction; $PCA_{trans}^{landing}$ – peak component acceleration of the stair landing in the transverse direction.

the landing PCAs in this direction and the corresponding PFAs were all below 100%. In addition, the landing PCAs in the transverse direction were 20–40% of their longitudinal counterparts during the base-isolated tests. In contrast, the landing accelerations were amplified notably, while the building was fixed at its base, with amplifications as high as 30%. In addition, the PCAs in the transverse direction exceeded their longitudinal counterparts by about 40–80%. The distinction of the acceleration responses between the base-isolated and fixed-base tests can be attributed to the period shift of the test building, because the predominant long-period response of the BI building was less likely to excite the higher frequency stair torsional response than the response of the fixed-base building.

5.2.2. Displacement response. The displacement responses of the stairs were obtained by double-integrating the measured stair acceleration responses. Because the acceleration responses of the stairs and the building were measured using separate data acquisition systems with different sampling frequencies (i.e., 200 Hz for the building and 240 Hz for the stairs), the acceleration responses of the stairs were resampled at 200 Hz and time-synchronized with the building responses for calculating the stair displacements relative to the building. The relative displacements were then filtered using a fourth-order Butterworth filter with band-pass frequencies between 0.25 and 25 Hz. It is noted, however, that permanent displacements (low frequency drifts) accumulated by the stairs are not captured when displacement responses are obtained through the double-integration method.

Figure 14 shows the displacement time histories of the stair landing at level 2 relative to the lower (second) floor of the building as well as the interstory drift response of level 2 during test FB-3. Test FB-3 is selected because level 2 achieved the largest interstory drift demands (about 1%) prior to the onset of severe damage to the stair at this level. The time instances of the positive (denoted as red circles) and negative (denoted as blue diamond) peak interstory drift responses are identified and then correlated with the landing displacement responses. It is also noted that landing drift ratios are presented in these plots, which are calculated as the ratios between the landing horizontal displacements and the height of the landing (half the story height).

As shown in Figure 14, the longitudinal landing displacements at the two corners differed significantly. While the peak relative displacement was 17 mm (corresponding to a landing drift ratio of 0.8% or a peak interstory drift of 41%) on the north corner, the response was much smaller at the south corner of the landing and the peaks did not coincide with those of the interstory drift response. The fact that the transverse displacement of the landing was as large as the longitudinal counterpart at the north corner indicates that the stair landing twisted appreciably. Figure 14 also presents the orbital plots of
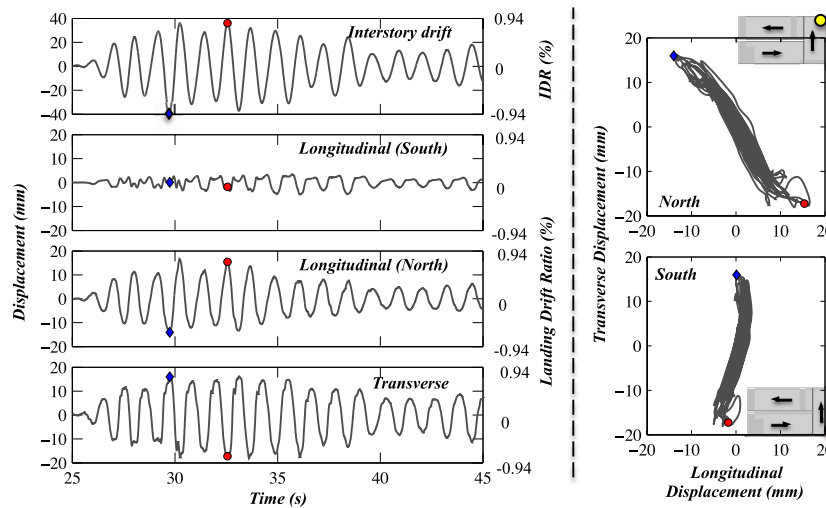
Figure 14. Displacement time histories of the stair landing at level 2 relative to the lower floor during test FB-3 (note: red dot denotes the positive interstory drift peak and blue dot denotes the negative peak).

Table VII. Peak responses of the landing displacement relative to the lower floor and the upper flight-to-slab connection deformation of the stair at level 2.

Test name	$PIDR$ (%)	PID (mm)	$\Delta_{long}^{landing}$ (mm)	$\dfrac{\Delta_{long}^{landing}}{PID}$ (%)	$\Delta_{trans}^{landing}$ (mm)	$\dfrac{\Delta_{trans}^{landing}}{PID}$ (%)	$\Delta^{connection}$ (mm)	$\dfrac{\Delta^{connection}}{PID}$ (%)
BI-1:CNP100	0.08	3.5	0.9	26	0.9	26	–	–
BI-2:LAC100	0.10	4.3	1.0	22	0.8	18	–	–
BI-3:LAC100	0.11	4.5	1.0	21	0.7	16	–	–
BI-4:SP100	0.10	4.2	1.4	33	1.4	32	–	–
BI-5:ICA50	0.09	3.9	0.7	19	0.7	19	–	–
BI-6:ICA100	0.19	8.0	1.5	18	1.4	17	–	–
BI-7:ICA140	0.32	13.6	3.2	24	2.4	18	–	–
FB-1:CNP100	0.47	19.8	9.9	50	9.9	50	6.3	32
FB-2:LAC100	0.55	23.8	10.3	43	11.3	48	7.8	33
FB-3:ICA50	0.94	40.2	16.6	41	18.1	45	13.3	33

Notes: $PIDR$ – peak interstory drift ratio; PID – peak interstory drift; $\Delta_{long}^{landing}$ – peak longitudinal landing displacement relative to the lower floor; $\Delta_{trans}^{landing}$ – peak transverse landing displacement relative to the lower floor; $\Delta^{connection}$ – peak deformation of the upper flight-to-building connection (data not available in the base-isolated tests).

the displacement responses at the two corners of the landing. Correlation of the stair displacement responses in the two horizontal directions of the building further corroborates the landing torsional response. It is clearly shown in the orbital plots that while the relative displacement was primarily in the transverse direction at the south corner, the north corner of the landing moved diagonally as the amplitudes of the relative displacements were similar in the two orthogonal directions. This can be attributed to the fact that the upper flight-to-building connection was much more deformable than the lower flight-to-building connection, and therefore allowed the landing to move in a torsional mode against the landing-to-lower flight connection.

5.2.3. Connection deformation response. Figure 15 shows the longitudinal connection deformation responses of the stair at level 2 during test FB-3. These responses were measured directly using displacement transducers (D-L-1 to D-L-8), and they were filtered with a low-pass fourth-order Butterworth filter with a corner frequency at 25 Hz. As shown in the figure, the deformation of the upper
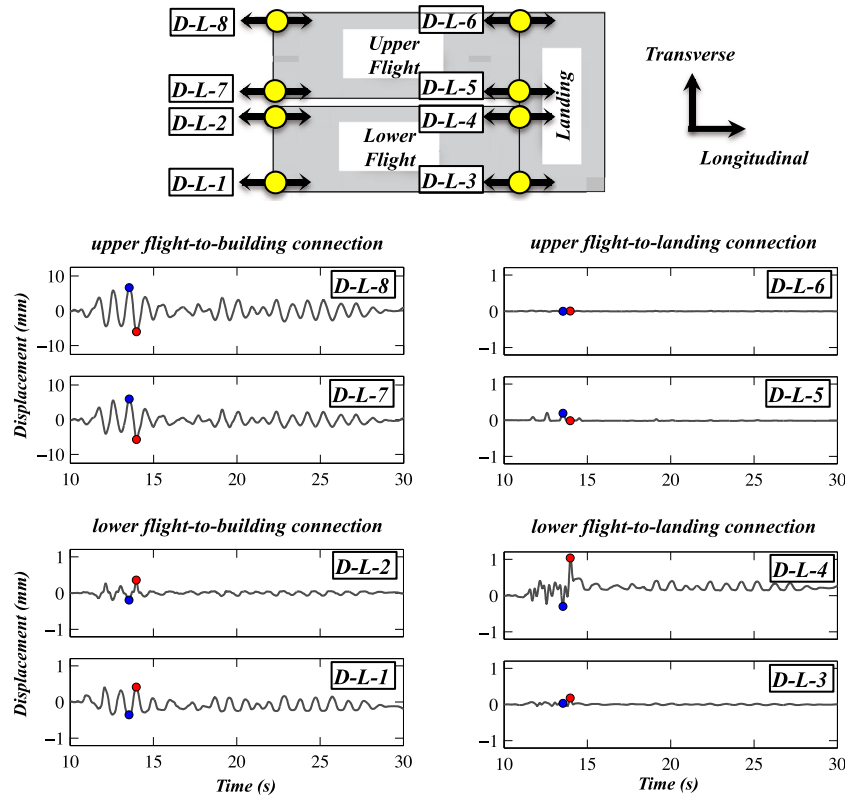
Figure 15. Longitudinal connection deformation time histories of the stair at level 2 during test FB-3 (note: red dot denotes the positive interstory drift peak and blue dot denotes the negative peak).

flight-to-building connection was about 16 mm (about 30% of the peak interstory drift at level 2) and were much larger than that of the lower flight-to-building connection. It is noted, however, that D-L-1 failed to record the connection deformation shortly after the negative peak interstory drift occurred. In addition, comparison of the connection deformation responses to the peak interstory drifts suggests that the two flight-to-building connection deformation responses were in the complete reversed direction. The flight-to-landing connection deformations were also small compared with those of the upper flight-to-building connection. It is noteworthy that the repair action R-II (Figure 10(b)) of the upper flight-to-slab connection for the stair at level 2 immediately following test FB-4 modified the original deformation mechanism of the stair system. Absent the intended yielding mechanism at the upper flight-to-building connection because of the repair, the relative deformation of the other connections increased significantly during the last two FB tests and led to plastic yielding of the connection plate between the lower flight and the landing during test FB-5 (Figure 9(d)).

5.2.4. Discussion of the displacement responses of the stair system. Prior to the onset of severe damage to the stair, the measured responses indicate that deformation of the stair at level 2 is characterized by the landing torsional movement as well as the upper flight-to-building connection deformation. Table VII summarizes the peak landing displacements relative to the lower floor and the upper flight-to-building connection deformation at level 2 in all base-isolated and the first three fixed-base tests. These responses are compared with the associated peak interstory drifts. It is observed that the peak landing displacements relative to the lower floor were very similar in the two orthogonal directions in all these tests. While the displacements were about 20–30% those of the interstory drifts in the BI tests, the ratio increased to 45–50% in the first three FB tests. In addition, the upper flight to building connection deformation consistently accounted for more than 30% of the interstory drift in each of the first three FB tests.

6. CONCLUSIONS

A prefabricated steel stair system was installed within a full-scale five-story reinforced concrete building and was subsequently tested with the building in a shake table test program. The building was subjected to a suite of uni-directional earthquake motions and low-amplitude WN base excitations, first, while the building was isolated at its base and subsequently fixed to the shake table platen. These system-level tests, for the first time, allowed investigation of the seismic behavior of stair systems under realistic installation conditions and earthquake motions. Coincident with the seismic tests, low-amplitude white noise base excitations were applied to the test building. These data are used to perform modal identification of the stair system at various stages of the test program. Important findings regarding the dynamic characteristics and seismic response of the prefabricated steel stairs are summarized as follows:

(1) The modal identification results indicate that the first and second vibrational modes of the stairs both correspond to the global torsional vibration of the stair systems with frequencies of 8.9 and 11.1 Hz, respectively. As a result, the stairs observed considerable acceleration and displacement responses in the transverse-to-flight direction, even when loading was imposed entirely in the parallel-to-flight direction. The stair landing displacements were comparable in the two directions, and its accelerations in the transverse-to-flight direction was observed to be even larger than those in the parallel-to-flight (loading) direction.

(2) During the seismic tests, severe damage to the stairs was detected at all levels except level 5. The most severe damage to the stairs consistently initiated in the form of vertical weld fracture of connection angles between the uppers flights and the slab embeds, with the associated PIDRs ranging from 0.74% to 2.64%. Safe egress from the building was compromised even when the associated drift demands (PIDRs of 0.74% and 1.41%) were much lower than the design performance target of the building (PIDR of 2.5%).

(3) Consistent with the findings in previous studies, the seismic performance of stair systems is highly dependent on the deformability of their connections to the building, and in the case of scissor stairs, the torsional deformability of the system is particularly important. Prior to severe damage to the stairs in the present tests, the deformation of the upper flight-to-building connection accommodated more than 30% of the interstory drift demands, while the torsional deformation of the landing was about 50% of that of the interstory drift demands.

(4) As a result of predominantly torsional movement, the stair system observed considerable out-of-plane (transverse) forces and deformations of similar amplitudes to those imposed along the in-plane (longitudinal) direction, despite the uni-directional seismic input excitations to the test building.

The present system-level test data (building outfitted with stairs and other nonstructural components and systems) provide unique opportunities for calibrating numerical models and subsequent parametric studies to further investigate the response of the critical egress system offered by prefabricated steel stairs.

REFERENCES

1. ICC. *International building code*, International Code Council: Washington, D.C, 2012.
2. Bull DK. *Stair and Access Ramps Between Floors in Multi-storey Buildings*, A report of the Canterbury Earthquakes Royal Commission: Christchurch, New Zealand, 2011.
3. Kam WY, Pampanin S. The seismic performance of RC buildings in the 22 February 2011 Christchurch earthquake. *Structural Concrete* 2011; **12**4:223–233.
4. Li B, Mosalam KM. Seismic performance of reinforced-concrete stairways during the 2008 Wenchuan earthquake. *ASCE Journal of Performance of Constructed Facilities* 2013; **27**6:721–730.
5. Roha C, Axley JW, Bertero VV. The performance of stairways in earthquakes. *Technical Report UCB/EERC-82/15*, Earthquake Engineering Research Center, University of California, Berkeley: Berkeley, CA, 1982.
6. ASCE 7–10. *Minimum Design Loads for Buildings and Other Structures*, American Society of Civil Engineers: Reston, VA, 2010.
7. Higgins C. Prefabricated steel stair performance under combined seismic and gravity loads. *ASCE Journal of Structural Engineering* 2009; **135**2:122–129.
8. Simmons PW, Bull DK. The safety of single storey straight stairflights with mid-height landings under simulated seismic displacements. *Technical Report Research Report 2000-09*, Department of Civil Engineering, University of Cantebury: Christchurch, New Zealand, 2000.
9. Cosenza E, Verderame GM, Zambrano A. Seismic performance of stairs in the existing reinforced concrete building, *Proceedings of the 14th World Conference on Earthquake Engineering*: Beijing, China, October 12–17, 2008.
10. Tegos IA, Panoskaltsis VP, Tegou SD. Analysis and design of staircases against seismic loadings, *Proceedings of 4th Eccomas Thematic Conference on computational methods in structural dynamics and earthquake engineering*: Kos Island, Greece, June 12–14, 2013.
11. Van Den Einde L, Restrepo JI, Conte JP, Luco E, Seible F, Filiatrault A, Clark A, Johnson A, Gram M, Kusner D, Thoen B. Development of the George E. Brown Jr. network for earthquake engineering simulation (NEES) large high performance outdoor shake table at the University of California, San Diego, *Proceedings of the 13th world conference on earthquake engineering*: Vancouver, B.C., Canada, August 1–6, 2004.
12. Chen M, Pantoli E, Wang X, Astroza R, Ebrahimian H, Mintz S, Hutchinson T, Conte J, Restrepo J, Meacham B, Kim J, Park H. BNCS Report #1: Full-scale structural and nonstructural building system performance during earthquakes and post-earthquake fire – specimen design, construction, and test protocol. *Technical Report SSRP-2013/09*, Department of Structural Engineering, University of California, San Diego: La Jolla, CA, 2013.
13. Hutchinson TC, Restrepo JI, Conte JP, Meacham B. Shake table testing of a full-scale five-story building: performance of the major nonstructural components–overview, *Proceedings of ASCE 2013 Structures Congress*: Pittsburg, PA, May 2–4, 2013; 1472–1484.
14. Pantoli E, Chen M, Wang X, Astroza R, Ebrahimian H, Mintz S, Hutchinson T, Conte J, Restrepo J, Meacham B, Kim J, Park H. BNCS Report #2: Full-scale structural and nonstructural building system performance during earthquakes and post-earthquake fire – test results. *Technical Report SSRP-2013/10*, Department of Structural Engineering, University of California, San Diego: La Jolla, CA, 2013.
15. Wang X, Pantoli E, Hutchinson C, Restrepo J, Wood R, Hoehler M, Grzesik P, Sesma F. Seismic performance of cold-formed steel wall systems in a full-scale building. *Journal of Structural Engineering* 2015. DOI: 10.1061/(ASCE)ST.1943-541X.0001245.
16. Kuntz GL, Browning J. Reduction of column yielding during earthquakes for reinforced concrete frames. *ACI Structural Journal* 2003; **100**5:573-580.
17. Moehle JP, Hooper JD, Lubke CD. Seismic design of reinforced concrete special moment frames: a guide for practicing engineers. *Technical Report NIST GCR 8-917-1*, National Institute of Standards and Technology: Gaithersburg, MD, 2008.
18. Pantoli E, Chen M, Hutchinson T, Restrepo J. BNCS Report #3: Full-scale structural and nonstructural building system performance during earthquakes and post-earthquake fire – camera and analog sensor details. *Technical Report SSRP-2013/11*, Department of Structural Engineering, University of California, San Diego: La Jolla, CA, 2013.
19. Van Overschee P, De Moor B. *Subspace Identification for Linear Systems: Theory, Implementation, Applications*, Kluwer academic publishers: Boston, MA, 1996.
20. Astroza R, Ebrahimian H, Conte JP, Restrepo JI, Hutchinson TC. System identification of a full-scale five-story reinforced concrete building tested on the NEES-UCSD shake table. *Submitted to Structural Control and Health Monitoring*.
21. Belleri A, Moaveni B, Restrepo J. Damage assessment through structural identification of a three-story large-scale precast concrete structure. *Earthquake Engineering and Structural Dynamics* 2014; **43**1:61–76.
22. Moaveni B, He X, Conte JP, Restrepo JI, Panagiotou M. System identification study of a 7-story full-scale building slice tested on the UCSD-NEES shake table. *Journal of Structural Engineering* 2010; **137**6:705–717.
23. Downing SD, Socie DF. Simple rainflow counting algorithms. *International Journal of Fatigue* 1982; **4**1:31–40.
24. Imregun M, Ewins DJ. Realisation of complex mode shapes, *Proceedings of the 11th International Modal Analysis Conference*: Kissimmee, FL, Feb 1–4, 1993; 1303–1309.
25. Wang X, Hutchinson TC, Conte JP, Restrepo JI. Computational assessment of seismic behavior of prefabricated steel stairs. *In Preparation* 2015.

26. Allemang RJ, Brown DL. A correlation coefficient for modal vector analysis, *Proceedings of the 1st International Modal Analysis Conference*: Orlando, FL, Nov 8–10, 1982; 110–116.
27. ACI. *Building Code Requirements for Structural Concrete and Commentary*, American Concrete Institute: Farmington Hills, MI, 2008.